

# Simple flow meter and viscometer of high accuracy for gases

Robert F Berg

Process Measurements Division, National Institute of Standards and Technology,  
Gaithersburg, MD 20899-8364, USA

Received 21 September 2004

Published 6 January 2005

Online at [stacks.iop.org/Met/42/11](http://stacks.iop.org/Met/42/11)

## Abstract

A model and supporting measurements are presented for the laminar flow of gases through a long capillary with a circular cross section. Using the model with a coil of quartz capillary of known dimensions yields the flow rates of a gas of known viscosity with an uncertainty of 0.04%. Alternatively, combining the model and capillary with an independent measurement of flow rate yields the gas viscosity with similar uncertainty. The model corrects the Hagen–Poiseuille equation for (1) departures from ideal gas behaviour, (2) slip at the capillary walls, (3) kinetic energy changes at the capillary entrance, (4) gas expansion along the length of the capillary, (5) viscous heating and (6) centrifugal effects that occur when a long capillary is coiled to fit into a small volume. The corrections are expressed in terms of familiar dimensionless parameters.

Measurements near room temperature using helium, nitrogen, argon, propane and sulfur hexafluoride demonstrated that the model describes the flow rates of gases with widely varying properties at Reynolds numbers as large as 1000. Combining the flow rates with independent measurements of the capillary length and radius yielded new absolute viscosity values for the five gases at 25 °C with an uncertainty of 0.04%. This small uncertainty was verified independently by comparing the result for the viscosity of helium to recent calculations using quantum mechanics and statistical mechanics. The present results allow one to construct a flow meter or viscometer of similar accuracy with no measurement of the capillary radius and only a nominal measurement of the capillary length.

## 1. Introduction

The impedance of a capillary used as a flow meter or a viscometer is calculated approximately with the Hagen–Poiseuille equation [1],

$$Q_0 = \frac{\pi R^4 (P_1 - P_2)}{8\eta L}. \quad (1)$$

Equation (1) relates the volume flow rate  $Q_0$  of an incompressible liquid with viscosity  $\eta$  to the internal radius  $R$  and length  $L$  of the capillary. ( $P_1$  and  $P_2$  are the input and output pressures.) The persistence of laminar flow in a capillary allows the use of equation (1) beyond creeping flow to Reynolds numbers ( $Re$ ) as large as 2000.

This article describes an accurate gas flow model that includes six corrections to equation (1). Using the model

with a capillary of known dimensions yields the flow rate of a gas of known viscosity with an uncertainty of 0.04%. Alternatively, combining the model and capillary with an independent measurement of flow rate yields the gas viscosity with a similar uncertainty. Measurements using a coil of quartz capillary demonstrated both applications.

Figure 1 shows the results for the flow rates of five gases. Here, the model used literature values for the viscosities and nominal values for the length and radius of a quartz capillary. The nominal length  $L_{\text{nom}}$  was determined with a tape measure, and  $R_{\text{nom}}$  was adjusted so that the average offset for nitrogen was zero. Using the same value of  $R_{\text{nom}}$  for the other gases caused flow-independent offsets, but those offsets are within the uncertainties of literature viscosity values. With the exception of helium, the model required no other

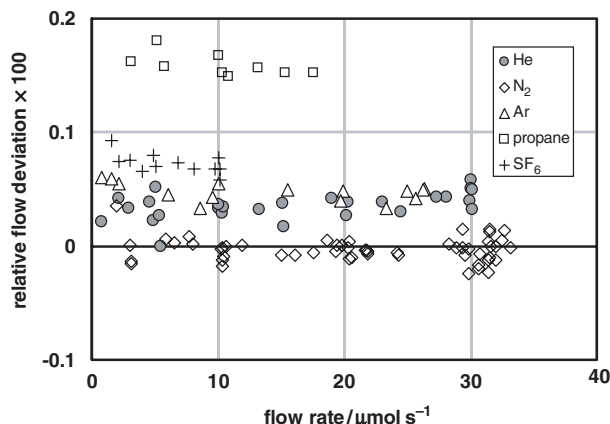


**Figure 1.** Relative flow deviations  $(\dot{n}_{\text{QCFM}}/\dot{n}_{\text{primary}} - 1) \times 100$ , where  $\dot{n}_{\text{QCFM}}$  is the modelled flow rate in a coiled QCFM (medium flow element in [2]) and  $\dot{n}_{\text{primary}}$  is the flow rate measured with a primary flow standard. The effective capillary radius was defined to minimize the deviations for nitrogen. The differences among the five gases are within the uncertainties of published viscosity values. Flow rates with large centrifugal corrections ( $De > 16$ , equation (12)) are not shown.

adjustable parameter besides  $R_{\text{nom}}$ . (Helium's momentum accommodation coefficient was determined from additional measurements.)

The offsets allow improved estimates of gas viscosity ratios with a precision of 0.01%. Combining those ratios with accurate, independent measurements of  $R$  and  $L$  yielded new viscosity values for the five gases with an uncertainty of 0.04%. This small uncertainty was verified by comparing the result for the viscosity of helium to recent calculations using quantum mechanics and statistical mechanics.

A previous paper [2] described the construction of the quartz capillary flow meter (QCFM) used for the present measurements, and it gave algorithms for constructing a similar flow meter and for implementing the model at  $De < 16$ . This paper gives the model's derivation and extends it to  $De = 100$ . It also demonstrates the flow meter's performance up to  $De = 67$ , and describes the independent measurements of  $R$  and  $L$  that converted the flow meter into an absolute viscometer. Section 2 gives a brief description of the instrument. Section 3 outlines the model and refers to appendix A for details of the derivation. Section 4 gives experimental results for the five gases.

## 2. The instrument

The QCFM is a portable transfer standard used to compare primary flow meters at the National Institute of Standards and Technology to those elsewhere. It is a laminar flow meter, which means that it uses pressure measurements to determine the rate of non-turbulent flow through a flow element made from quartz capillary tubing manufactured for gas chromatography. The present measurements used an element with an internal radius  $R = 157 \mu\text{m}$  and a length  $L = 6.4 \text{ m}$  arranged in a 200 mm diameter coil. Commercial pressure gauges based on a vibrating quartz flexure measured the input and output pressures  $P_1$  and  $P_2$  in the range from 28 kPa to 310 kPa. 'Taring' the entrance gauge to the exit gauge

at zero flow rate caused the uncertainty of the difference  $P_1 - P_2$  to be limited only by the gauge reproducibility. A temperature-controlled air bath (25 °C) housed the flow element, the pressure gauges and two platinum resistance thermometers, all of which were attached to an internal frame. Reference [2] gives complete details of the flow meter's operation and construction.

An accurate measurement of  $R$  was possible because the commercially available quartz capillary offers two advantages beyond the dimensional stability of quartz. The first is its transparency, which allowed an easy measurement of the length of a bead of mercury placed in the capillary. Combining that length with weight measurements yielded the cross-sectional area of the capillary. The second advantage is the tightly controlled cross section due to the capillary drawing technique that is similar to that used to manufacture optical fibres. The value of  $R$  obtained from the cross-sectional area thus had negligible errors due to geometric imperfections.

An accurate measurement of  $L$  was surprisingly difficult. The value obtained with an interferometric bench differed from  $L_{\text{nom}}$  because the tape measure used to obtain  $L_{\text{nom}}$  had a significant error. By using the present viscosity values, the reader can avoid this difficulty when constructing a similar flow meter or viscometer. Combining a nominal length measurement with one of the present viscosity values and an independent measurement of flow rate of the corresponding gas will yield an accurate value of  $R^4/L$ . No measurement of  $R$  would be required.

The independent measurements of flow rate were made by a primary standard that combined the gas equation of state with measurements of pressure, temperature, volume and time. Its largest moving part was a piston of diameter  $D$  that moved into or out of an oil-filled chamber. Consequently, gas flowed out of or into a metal bellows contained in the oil chamber. A displacement  $\Delta x$  of the piston out of the oil chamber increased the bellows volume by  $(\pi D^2/4)\Delta x$ . A commercial laser interferometer measured the piston's displacement. Reference [3] describes the standard in detail.

## 3. Hydrodynamic model

The model for the molar flow rate  $\dot{n}$  is

$$\dot{n} = \dot{n}_0 \left[ 1 + g_{\text{virial}}(P_1, P_2) + 4K_{\text{slip}}Kn + \frac{K_{\text{ent}} R}{16 L} Re + \left( \frac{K_{\text{exp}}}{8} + \frac{K_{\text{therm}}}{16} \right) \frac{R}{L} Re \ln \left( \frac{P_2}{P_1} \right) \right] f_{\text{cent}}(De, \delta). \quad (2)$$

Here  $Re$  is the Reynolds number,  $Kn$  the Knudsen number,  $De$  the Dean number and  $\delta$  is the ratio of the capillary internal radius to the coil radius of curvature. The function  $g_{\text{virial}}$  for non-ideal gas behaviour is described in appendix A, and the constants  $K_{\text{slip}}$ ,  $K_{\text{ent}}$ ,  $K_{\text{exp}}$  and  $K_{\text{therm}}$  are determined independently.

The model is implemented in three parts. The first part combines Poiseuille's Law and the ideal gas law to approximate the flow through a straight capillary as  $\dot{n}_0$ ; section 3.1 briefly reviews the derivation of  $\dot{n}_0$ . The second part, contained in the large bracket in equation (2), corrects  $\dot{n}_0$  for five effects that are present in both straight and

curved capillaries; section 3.2 discusses their significance and appendix A gives their derivations. The third part uses the function  $f_{\text{cent}}$  to correct for centrifugal effects; section 3.3 discusses  $f_{\text{cent}}$  and appendix B discusses errors of  $f_{\text{cent}}$  due to imperfections of the capillary's cross section.

The model's first five corrections account for (1) departures from the ideal gas law, (2) slip at the capillary walls, (3) kinetic energy changes at the capillary entrance, (4) gas expansion along the length of the capillary and (5) viscous heating. Models including some of these phenomena have been used elsewhere (see the references in [4]), but the present model is the first to include all five corrections in accurate form. The correction for non-ideal gas behaviour is improved with second-order virials of pressure and viscosity, and the slip correction is improved with modern results that relate the slip length to the viscosity. The corrections for gas expansion and viscous heating rely on theoretical results for gas capillary viscometers described in two remarkable papers by van den Berg *et al* [5, 6]. All five corrections are expressed in terms of familiar dimensionless parameters.

Making the capillary longer reduces the third, fourth and fifth corrections because they are proportional to  $(R/L)Re$ . Coiling such a capillary to fit into a small volume improves the instrument's temperature control and convenience. Therefore, the model's sixth correction is for the centrifugal effects of the curved capillary. The centrifugal correction received careful attention because it can be ten times larger than the other corrections combined. Previous analytical models of centrifugal effects in a curved capillary were used where possible. Larrain and Bonilla's model [7] is reliable but limited to Dean numbers  $De < 16$ . Van Dyke's extension of their model to larger  $De$  [8] was known to fail for  $De > 120$ , but its accuracy in the intermediate range  $16 < De < 120$  was unclear. The present model relies on recent numerical calculations by Fan [9, 10] which deviate from van Dyke's model in the intermediate range by as much as 0.7%.

### 3.1. Poiseuille flow of an ideal gas

The ideal flow  $\dot{n}_0$  can be derived [1] from the differential form of Poiseuille's Law,

$$dP = -\frac{8\eta Q}{\pi R^4} dz, \quad (3)$$

where  $Q$  is the volume flow rate at position  $z$  along the capillary's length. After assuming that the gas is isothermal and ideal and integrating along the capillary, one obtains

$$Q_1 = Q_0 \left( \frac{1 + P_2/P_1}{2} \right), \quad (4)$$

where  $Q_1$  is the volume flow rate at the capillary's entrance, and  $Q_0$  describes the Poiseuille flow of an *incompressible* fluid according to equation (1). The bracket of equation (4) contains the model's main adjustment for compressibility. It is approximately 1 at low flow rates and approaches  $\frac{1}{2}$  at the largest flow rates. Combining equations (3) and (4) and multiplying  $Q_1$  by  $P_1/(R_{\text{gas}}T)$  yields the ideal gas molar flow rate

$$\dot{n}_0 = \frac{\pi R^4 (P_1^2 - P_2^2)}{16\eta(T, 0)LR_{\text{gas}}T}, \quad (5)$$

where  $R_{\text{gas}}$  is the universal gas constant and  $\eta(T, 0)$  is the viscosity evaluated at temperature  $T$  in the limit of zero pressure.

### 3.2. Five corrections to flow through a straight capillary

The five correction terms in the large bracket in equation (2) have the following significance.

1. The function  $g_{\text{virial}}$  corrects for the density dependence of viscosity and deviations of the gas compressibility from the ideal gas law.
2. The term proportional to  $K_{\text{slip}}$  corrects for slip at the capillary's walls, which increases the flow rate. This effect is proportional to the Knudsen number,  $Kn$ , which is the gas mean free path divided by the capillary radius.
3. The term proportional to  $K_{\text{ent}}$  corrects for the increase of kinetic energy that occurs near the capillary's entrance. The increase occurs because the gas's average velocity increases as it flows into the entrance of the capillary. It increases further as the flow profile changes from nearly uniform at the entrance to nearly parabolic farther downstream. The resulting pressure drop decreases the flow rate.
4. The term proportional to  $K_{\text{exp}}$  corrects for gas expansion along the capillary, which also increases the kinetic energy and decreases the flow rate.
5. The term proportional to  $K_{\text{therm}}$  accounts for the radial temperature distribution of the gas in the capillary, which results from the combination of heating due to viscous friction and cooling due to gas expansion. These two effects nearly cancel, so that the temperature of the gas in the middle of the capillary is only slightly cooler than that of the wall.

Appendix A derives the five corrections, and table 1 gives the values of the correction coefficients.

The correction terms in equation (2) depend on the Reynolds number  $Re$ , Knudsen number  $Kn$ , the aspect ratio  $R/L$  and the pressure ratio  $P_2/P_1$ . The density dependence of viscosity causes  $Re$  to vary slightly along the length of the capillary. Here, we will use the constant value defined by

$$Re \equiv \frac{2M\dot{n}}{\pi R\eta(T, \bar{P})}, \quad (6)$$

where the molar mass is  $M$ , and the pressure averaged along the length of the capillary is [4]

$$\bar{P} \equiv \frac{1}{L} \int_0^L P(z) dz \cong \frac{2}{3} \left( \frac{P_1^3 - P_2^3}{P_1^2 - P_2^2} \right). \quad (7)$$

**Table 1.** Correction coefficients in the model. The value of  $K_{\text{therm}}$ , which is gas dependent, is for nitrogen. The value of  $K_{\text{slip}}$  describes the momentum accommodation at the gas capillary interface; in the present measurements, only helium deviated from  $K_{\text{slip}} = 1.00$ .

Coefficient	Value	Reference
$K_{\text{slip}}$	+1.00	[11, 12, this work]
$K_{\text{ent}}$	-1.14	[1]
$K_{\text{exp}}$	+1.00	[5]
$K_{\text{therm}}(\text{N}_2)$	-0.26	[6, this work]

The density dependence of viscosity is so weak, and the correction terms in equation (2) are so small, that using equation (6) to approximate  $Re$  by a constant has adequate accuracy.

The Knudsen number varies greatly along the length of the capillary. Appendix A shows that a suitable constant definition is

$$Kn \equiv \frac{\lambda_{1/2}}{R} = \frac{1}{R} \left( \frac{2R_{\text{gas}}T}{M} \right)^{1/2} \frac{\eta_{1/2}}{P_{1/2}}, \quad (8)$$

where  $\lambda_{1/2}$  is the gas mean free path defined for the ‘half’ quantities given by

$$P_{1/2} \equiv \frac{P_1 + P_2}{2} \quad \text{and} \quad \eta_{1/2} \equiv \eta(P_{1/2}). \quad (9)$$

### 3.3. Centrifugal correction

Consider a straight capillary whose input and output pressures,  $P_1$  and  $P_2$ , drive a molar flow rate  $\dot{n}_{\text{straight}}$ . Curving the capillary into a coil of radius  $R_{\text{curve}}$  while holding constant  $P_1$  and  $P_2$  gives rise to a secondary flow that is transverse to the original axial flow. The additional dissipation decreases the molar flow rate to

$$\dot{n} = \dot{n}_{\text{straight}} f_{\text{cent}}(De, \delta), \quad (10)$$

where

$$\delta \equiv \frac{R}{R_{\text{curve}}} \quad (11)$$

is the curvature ratio and

$$De \equiv Re \delta^{1/2} \quad (12)$$

is the Dean number.

Figure 2 plots the centrifugal function  $f_{\text{cent}}(De, \delta)$ , which is the model’s largest correction for  $De > 16$ . It was first calculated by Dean [13, 14] for  $De < 10$  in the limit of infinitesimal  $\delta$ . Larrain and Bonilla [7] used a double expansion to calculate  $f_{\text{cent}}(De, \delta)$  to an uncertainty of 0.01%

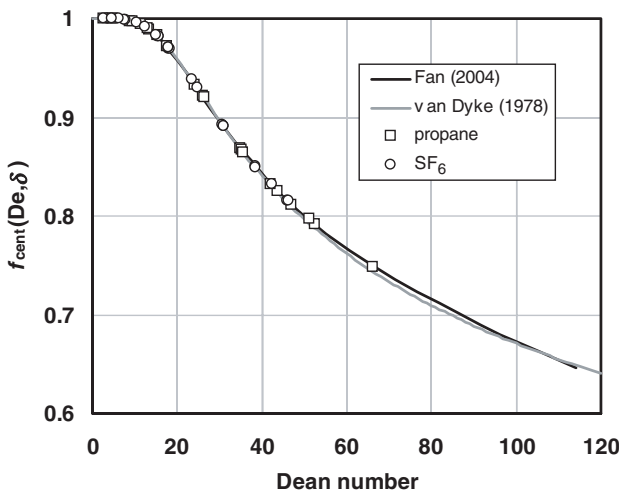


**Figure 2.** The centrifugal correction  $f_{\text{cent}}$  as a function of  $De$ . The measurements, with propane and  $\text{SF}_6$ , and the numerical results by Fan [9, 10] disagree with van Dyke’s analytical theory [8] by as much as 0.7%. The measurements used the medium element of the QCFM described in [2].

for  $De < 16$ . Van Dyke [8] used an Euler expansion to extend  $f_{\text{cent}}(De, 0)$  to arbitrarily large  $De$ , but its asymptotic dependence of  $De^{1/4}$  made his solution controversial. (See the review by Berger *et al* [15].) Numerical calculations later showed that van Dyke’s expression was at least approximately valid up to  $De = 100$ , but not higher [16].

The deviation plot of figure 3 demonstrates that the present measurements and recent numerical results by Fan [9, 10] are in agreement for  $De < 67$ . In this range, both differ from van Dyke’s result for  $f_{\text{cent}}(De, 0)$  by as much as 0.7%. Recoiling the capillary reduced  $R_{\text{curve}}$  from 100 mm to 48 mm, which yielded a larger value of  $De$  for a given flow rate. Obtaining similar results with the smaller coil proved that the deviations from van Dyke’s result depend on  $De$  and not  $Re$ .

The experimental data of figure 3 were normalized to 1 at small  $De$ . Therefore, the uncertainty components are those present only at large  $De$ . They include uncertainty due to viscosity,

$$\left( \frac{u_{\dot{n}}}{\dot{n}} \right)_{\eta} = \left( \frac{De}{f_{\text{cent}}} \frac{\partial f_{\text{cent}}}{\partial De} \right) \frac{u_{\eta}}{\eta}, \quad (13)$$

uncertainty due to the coil radius,

$$\left( \frac{u_{\dot{n}}}{\dot{n}} \right)_{R_{\text{curve}}} = \frac{1}{2} \left( \frac{De}{f_{\text{cent}}} \frac{\partial f_{\text{cent}}}{\partial De} \right) \frac{u_{R_{\text{curve}}}}{R_{\text{curve}}} \quad (14)$$

and uncertainty due to the length  $L_{\text{straight}}$  of capillary that connected the coil to the pressure gauges [2],

$$\left( \frac{u_{\dot{n}}}{\dot{n}} \right)_{L_{\text{straight}}} \simeq (1 - f_{\text{cent}}) \frac{u_{L_{\text{straight}}}}{L}. \quad (15)$$

Small additional contributions come from variation of the capillary radius and ellipticity of the capillary cross section; they are discussed in section 3.4.

The present model expresses the centrifugal function as the product of three functions,

$$f_{\text{cent}}(De, \delta) = f_{\text{approx}}(De) g_{\text{curve}}(De, \delta) g_{\text{dev}}(De). \quad (16)$$

The function  $f_{\text{approx}}$  is a simple approximate description of van Dyke’s result,  $g_{\text{curve}}$  accounts for curvature effects for  $\delta > 0$  and  $g_{\text{dev}}$  represents deviations of Fan’s results (extrapolated to  $\delta = 0$ ) from  $f_{\text{approx}}$ . Appendix C gives explicit forms for the three functions.

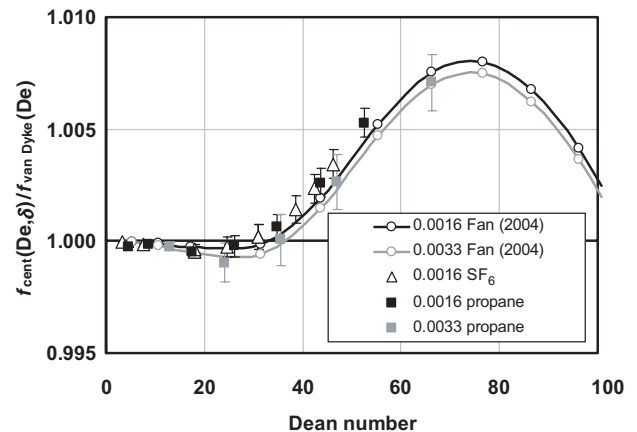


**Figure 3.** Deviations of the present measurements and Fan’s numerical results [9, 10] from van Dyke’s analytical theory [8]. The number given in the legend is the curvature ratio  $\delta$ . The text discusses the measurement uncertainties.

### 3.4. Neglected corrections

While equation (2) includes all significant effects, their interactions are neglected. (An example would be the influence of slip on the expansion correction. See Zohar *et al* [17], who generalized the results of van den Berg *et al* [5] to include slip.) The small values of the first five correction terms justify the neglect of interactions. For the present measurements, the largest,  $g_{\text{virial}}$ , was always less than 4% and the other four terms were less than 0.5%.

Other physical effects and a second-order interaction of the thermal effect with the large centrifugal correction were considered. The following list explains why they were neglected.

- *Exit flow.* Kinetic energy changes near the capillary's exit contribute negligibly to  $P_1 - P_2$  (see [2, 18]).
- *Bulk viscosity.* Gas expansion causes dissipation via the bulk viscosity  $\eta_B$ , which is larger for polyatomic gases. For SF<sub>6</sub> at 25 °C and 100 kPa,  $\eta_B$  exceeds the shear viscosity  $\eta$  by the factor

$$\frac{\eta_B}{\eta} \cong 4(\gamma - 1) \left(1 - \frac{3}{4}\gamma\right) \frac{P\tau}{\eta} \cong 345. \quad (17)$$

(This estimate was derived from equation (4.3.31) of [19]. Here  $\gamma$  is the heat capacity ratio and  $\tau$  is the molecular relaxation time obtained from [20]. The product  $P\tau \approx 75 \text{ mPa s}$  is approximately independent of temperature as well as pressure near ambient conditions [21].) The influence of bulk viscosity on the flow rate is measured by the ratio defined in [5]:

$$\frac{C_3}{C_2} \cong \frac{3}{4} \left(\frac{\eta_B}{\eta}\right) \left(\frac{R}{L}\right)^2 \left(\frac{P_1}{P_2}\right)^2 < 10^{-4}. \quad (18)$$

Thus, despite the large value of  $\eta_B/\eta$ , bulk viscosity required no correction to the flow rate.

- *Diffusion through quartz.* Diffusion of helium through the capillary's quartz walls was measured to be negligible [2].
- *Entrance length.* The velocity profile changes from uniform to nearly parabolic near the entrance of a straight capillary. The transition is half complete after a distance of approximately  $0.02ReR$  [22], which is less than 0.06% of the total capillary length for the present measurements. The entry length for centrifugal flow in a curved capillary is similar, at least for small  $De$  [15].
- *Expansion of the capillary radius.* A pressure  $P$  increases the capillary radius  $R$  by less than  $\Delta R = (P/E)(R^2/t)$ , where  $E$  and  $t$  are, respectively, the strength modulus and wall thickness of the capillary [23]. For the present measurements with the quartz capillary, the relative flow error  $4\Delta R/R$  was less than 0.006%.
- *Adsorption.* Adsorption will deposit on a smooth surface a liquid film whose thickness is approximately  $d = d_0/[\ln(P_S/P)]^{1/3}$ , where  $P_S$  is the saturation vapour pressure and  $d_0 \approx 1 \text{ nm}$  [24]. For the present measurements with propane,  $d < 1 \text{ nm}$ , and the corresponding decrease of the capillary radius would have decreased the flow by the relative amount  $4d/R$ , which is less than 0.003%.

- *Transverse convection.* The thermal correction assumes that the capillary is straight and that all radial heat transfer occurs without transverse convection. However, centrifugal effects cause transverse flows that reduce the thermal effect. The maximum velocity of transverse flow is  $[De^2/(36Re)]\langle v \rangle$  [7], where  $\langle v \rangle$  is the longitudinal velocity averaged over the cross section. A simple estimate based on this velocity predicts that transverse convective heat transfer will significantly reduce the thermal correction only when  $De > (288/Pr)^{1/2} \approx 20$ , where  $Pr$  is the Prandtl number. The resulting error is less than the thermal correction, which, for the present measurements, was always less than 0.03%.
- *Variation of the capillary radius.* See appendix B. The manufacturer specified the capillary radius to be constant to within 0.5%. Suppose the capillary flared linearly along its length, namely  $R(z) = R_0 + (z/L)\Delta R$ . At small  $De$ , the resulting flow error would be

$$\frac{\Delta \dot{n}}{\dot{n}} = \left(\frac{\Delta R}{R_0}\right)^2 < 0.003\%. \quad (19)$$

At large  $De$ , interaction of the linear flare with the centrifugal function would cause no error. However, a quadratic flare,  $R(z) = R_0 + 4(z/L)(1 - z/L)\Delta R$ , would cause a flow error of approximately

$$\frac{\Delta \dot{n}}{\dot{n}} \approx \left(\frac{De}{f_{\text{cent}}}\right) \left(\frac{\partial f_{\text{cent}}}{\partial De}\right) \langle \delta_R \rangle \leq \frac{1}{4} \frac{1}{6} \left(\frac{\Delta R}{R_0}\right) = 0.02\%. \quad (20)$$

- *Ellipticity of the capillary cross section.* See appendix B. The manufacturer specified the capillary flatness to be  $|\varepsilon| < 0.03$ , but micrometer measurements on a new coil of capillary stock agreed with the manufacturer's estimate that the true flatness was  $|\varepsilon| < 0.01$ . At small  $De$ , the resulting flow error would be

$$\frac{\Delta \dot{n}}{\dot{n}} = \frac{\varepsilon^2}{2} = 0.005\%. \quad (21)$$

At large  $De$ , interaction of the flatness with the centrifugal function would cause a relative error less than 0.1%. Cancellation due to random variations of the orientation of the ellipse within the coil probably reduced the error to less than 0.03%.

## 4. Gas properties

Measurements were obtained by flowing gas through the QCFM into a pressure–volume–temperature–time ( $PVTt$ ) primary flow standard. Previous papers give details of the QCFM [2] and the flow standard [3]. To decrease the scatter associated with pressure measurements, all of the measurements except those shown on figure 4 used an exit pressure  $P_2$  near 100 kPa. The following subsections describe the results for the viscosity and the gas–quartz momentum accommodation obtained from the measurements.

### 4.1. Momentum accommodation

The slip parameter can be written as  $K_{\text{slip}} = (2 - f_S)/f_S$ , where  $f_S$  is the tangential momentum accommodation coefficient.

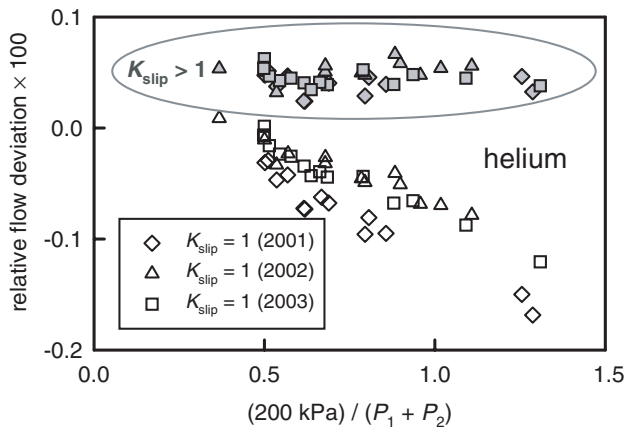


**Figure 4.** Relative flow deviations  $(\dot{n}_{\text{QCFM}}/\dot{n}_{\text{primary}} - 1) \times 100$  for helium. Assuming complete momentum accommodation ( $K_{\text{slip}} = 1$ , open points) introduced a pressure-dependent error. Allowing  $K_{\text{slip}} > 1$  (filled points) eliminated the time dependence as well as the pressure dependence.

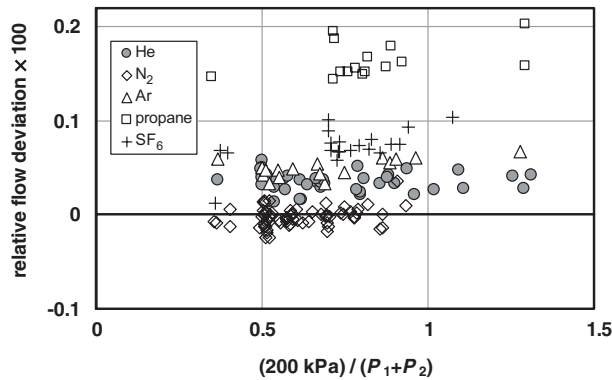


**Figure 5.** Relative flow deviations  $(\dot{n}_{\text{QCFM}}/\dot{n}_{\text{primary}} - 1) \times 100$  for five gases. The pressure independence of each gas's offset indicates an accurate choice for  $K_{\text{slip}}$ . Only helium required  $K_{\text{slip}} > 1$ .

The value of  $f_s$  depends on the gas, the capillary material and the capillary surface roughness relative to the mean free path  $\lambda$ . The value  $K_{\text{slip}} = f_s = 1.00$ , which corresponds to complete accommodation, was initially assumed for all five gases. This assumption was tested by varying the characteristic pressure  $P_{1/2}$  used in equation (8) independently of the flow rate. The assumption failed for helium only; figure 4 shows that  $K_{\text{slip}} > 1$  was required to eliminate pressure dependence from the helium results. This is understandable because helium's inertness decreases the likelihood of accommodation. The value of  $K_{\text{slip}}$  was time dependent, perhaps due to a slight roughening or contamination of the quartz surface. (The values during 2001, 2002 and 2003 were, respectively, 1.09, 1.19 and 1.14.) Regardless of the cause of the variation, the values of  $K_{\text{slip}}$  that eliminated the pressure dependence also eliminated the time dependence.

Figure 5 plots the measurement results for all five gases. The pressure independence of each gas's offset indicates an accurate choice for  $K_{\text{slip}}$ . Only helium required  $K_{\text{slip}} > 1$ ;  $K_{\text{slip}} = 1.00$  describes the other gases.

The present values of  $K_{\text{slip}}$  are smaller than the values found by Porodnov, Suetin, Borisov and co-workers [25, 26]. They measured the viscous flow ( $20 \text{ kPa} < P_{1/2} < 250 \text{ kPa}$ )

**Table 2.** Values of the low density viscosity  $\eta_0$  at  $25^\circ\text{C}$  obtained from the literature and from the present measurements: for optimum consistency, the measured values were derived only from flow measurements made with  $De < 20$  and  $P_2 \approx 100 \text{ kPa}$ , and the literature ratios were derived only from measurements made in a single laboratory (Vogel and co-workers). The absolute uncertainties of the last column correspond to a standard uncertainty of 0.37%.

Gas	$\eta_0$ (literature)/ ( $\mu\text{Pa s}$ )	$[C_{\text{N}_2}(\text{gas}) - 1] \times 100$	$\eta_0$ (this work)/ ( $\mu\text{Pa s}$ )
He	19.860 [31]	$-0.039 \pm 0.010$	$19.825 \pm 0.007$
N <sub>2</sub>	17.782 [31]	$0.000 \pm 0.010$	$17.757 \pm 0.007$
Ar	22.599 [31]	$-0.050 \pm 0.008$	$22.556 \pm 0.008$
C <sub>3</sub> H <sub>8</sub>	8.146 [28, 32]	$-0.162 \pm 0.010$	$8.121 \pm 0.003$
SF <sub>6</sub>	15.234 [28, 33]	$-0.076 \pm 0.009$	$15.201 \pm 0.006$

of He, N<sub>2</sub>, Ar and six other gases through glass capillaries and slits and found values of  $K_{\text{slip}}$  ranging from 1.1 to 1.5. However, they also found that increasing the roughness of the slits decreased both the value of  $K_{\text{slip}}$  and its gas dependence. The longer mean free paths (and perhaps smoother walls) in their capillaries may have caused their values of  $K_{\text{slip}}$  to be larger than the present values.

#### 4.2. Viscosity ratios

The model uses published values for the gas properties [27–34], which include the viscosity  $\eta_0$  (evaluated in the limit of zero pressure at  $25^\circ\text{C}$ ), the molar mass, the second virial pressure coefficient  $B_P$  and the thermal conductivity. It also uses the first temperature and density derivatives of viscosity to calculate the viscosity  $\eta(T, P)$  from  $T, P$  and  $\eta_0$ . For propane and SF<sub>6</sub>, the second derivatives are also used. The molar mass of SF<sub>6</sub> is 365 times that of helium, and the second virial coefficient of propane is 78 times that of nitrogen. The model correctly accounted for these large variations. The offsets between gases in figures 1 and 5 are *not* due to these variations because the offsets are independent of flow rate and pressure. Instead, they occurred because the published values for  $\eta_0$  have small errors that are less than their uncertainties.

The offsets in figure 1 yield improvements of the gas viscosity ratios. For example, the average offset for helium is greater than that for nitrogen by 0.04%. This implies that the helium/nitrogen viscosity ratio is less than its literature value by 0.04%. Data from figure 1 were averaged to construct the following ratios:

$$C_{\text{N}_2}(\text{gas}) \equiv \frac{(\eta_{\text{gas}}/\eta_{\text{N}_2})_{\text{this work}}}{(\eta_{\text{gas}}/\eta_{\text{N}_2})_{\text{literature}}} \quad (22)$$

All values of  $\eta_{\text{gas}}$  were evaluated in the limit of zero pressure and  $25^\circ\text{C}$ . Table 2 summarizes how the present viscosity ratios differ from their literature values.

#### 4.3. Absolute viscosities

Independent determinations of the capillary length and radius changed the capillary from a relative viscometer to an absolute viscometer. Before the flow measurements, the nominal value  $L_{\text{nom}}$  was measured with a tape measure, but the tape measure was later found to have an error of 0.03%. This error was negligible for the viscosity ratios due to cancellation, but it

was significant for the absolute viscosities. Therefore, an accurate value of  $L$  was obtained after the flow measurements by laying the capillary on a laser interferometric bench that included a travelling microscope attached to a retroreflector. Uncontrolled variation of the positions of the capillary ends caused variations in the measured value of  $L$ . The resulting uncertainty of 0.1 mm was nonetheless negligible.

The radius  $R$  was determined from the volume of the capillary. After the flow measurements were completed, pressurized nitrogen pushed mercury through the capillary until a mercury bead filled the entire capillary except for a few centimetres at the ends. The bead length was  $L_{\text{Hg}} = L - L_{\text{N}_2}$ , where the gas-filled length at the ends  $L_{\text{N}_2}$  was measured with a ruler with an uncertainty of 1 mm. The capillary was weighed before and after each of the three fillings. The buoyancy correction due to the difference between the density of mercury and the density of the balance calibration mass was negligible. After the first filling, a check for gas bubbles was performed by examining 20% of the bead surface under a microscope, and none was seen. The lack of bubbles was reasonable because the non-wetting of quartz by mercury discouraged the attachment of a gas bubble to the capillary wall, and the advancing bead would probably have swept out any such bubble.

Table 3 gives the three results for the radius  $R_{\text{volume}}$  determined from the bead volume  $\pi R_{\text{volume}}^2 L_{\text{Hg}}$ . The relative standard uncertainty  $u_{R1}$  of a single measurement is half the quadrature sum of the uncertainties due to the mercury density ( $u_{\rho}$ ), the mercury mass ( $u_M$ ) and the mercury bead length ( $u_{L_{\text{Hg}}}$ ). Its value,

$$\frac{u_{R1}}{R} = \frac{1}{2} \left[ \left( \frac{u_{\rho}}{\rho} \right)^2 + \left( \frac{u_M}{M} \right)^2 + \left( \frac{u_{L_{\text{Hg}}}}{L_{\text{Hg}}} \right)^2 \right] = \frac{0.001\%}{2} [4^2 + 2^2 + 16^2]^{1/2} = 0.008\% \quad (23)$$

is consistent with the scatter of the three measurements. The uncertainty of  $R_{\text{volume}}$  is thus  $(u_R/R) = (u_{R1}/R)/\sqrt{3} = 0.005\%$ .

Combining  $R_{\text{volume}}$  with the viscosity ratios in table 2 yields the absolute viscosity values,

$$\eta_{\text{gas}}(\text{this work}) = \left( \frac{R_{\text{volume}}}{R_{\text{nom}}} \right)^4 \left( \frac{L_{\text{nom}}}{L} \right) \times C_{\text{N}_2}(\text{gas}) \eta_{\text{gas}}(\text{literature}), \quad (24)$$

where the nominal radius  $R_{\text{nom}} = 156.925 \mu\text{m}$  was determined from  $L_{\text{nom}}$  and the literature value for the viscosity of nitrogen.

The last column of table 2 lists the resulting absolute values for  $\eta_{\text{gas}}$ . The standard ( $k = 1$ ) relative uncertainty is the quadrature sum of uncertainties from  $R_{\text{volume}}$ , temperature [2],

**Table 3.** Measurements of the capillary radius determined by filling the capillary with a mercury bead slightly shorter than the length of the capillary.

Measurement	Bead length $L_{\text{Hg}}/$ m	$R_{\text{volume}}/$ $\mu\text{m}$
1	6.089	156.882
2	6.174	156.875
3	6.146	156.898
Average		156.885

$C_{\text{N}_2}$ , the capillary radius variation  $\Delta R$  and the capillary flatness  $\varepsilon$ .

$$\begin{aligned} \frac{u_{\eta}}{\eta} &= \left[ \left( 4 \frac{u_R}{R} \right)^2 + \left( \left[ 1 + \left( \frac{T}{\eta} \frac{\partial \eta}{\partial T} \right) \right] \frac{u_T}{T} \right)^2 + \left( \frac{u_{C_{\text{N}_2}}}{C_{\text{N}_2}} \right)^2 \right. \\ &\quad \left. + \left( \frac{\Delta \dot{n}}{\dot{n}} \right)_{\Delta R}^2 + \left( \frac{\Delta \dot{n}}{\dot{n}} \right)_{\varepsilon}^2 \right]^{1/2} \\ &= [(4 \times 5)^2 + (1.69 \times 17)^2 + 10^2 + 5^2 + 5^2]^{1/2} 0.001\% \\ &= 0.037\%. \end{aligned} \quad (25)$$

Helium is of special interest because, as shown by Hurly and Moldover [35], its thermophysical properties can be calculated accurately with statistical mechanics and the helium–helium interatomic potential obtained *ab initio* from quantum mechanics. The uncertainty of the interatomic potential dominated their viscosity uncertainties. Since then, more accurate values of the potential have become available, particularly near 4.0 bohr [36, 37]. Hurly and Moldover [38] find that the new values shift the viscosity at 25 °C to  $\eta_0 = (19.823 \pm 0.006) \mu\text{Pa}\cdot\text{s}$ . (The uncertainty is a preliminary estimate.) The new theoretical value and the present experimental value agree to within their combined standard uncertainty of 0.05%.

## 5. Conclusion

The agreement of the *ab initio* value with the measured value for the viscosity of helium verified the small uncertainty in the determinations of  $R$  and  $L$  and of the hydrodynamic model for  $De < 16$ . An accurate *ab initio* value exists only for helium, but the flow rate independence shown in figure 1 supports the accuracy of the values measured for the other four gases also. At larger flow rates, the centrifugal correction due to coiling the capillary was large, and the agreement of Fan's numerical calculations with the measured flow rates shown in figure 3 verified the accuracy of the model for  $De < 67$ . Combining one of the present viscosity values with an independent measurement of flow rate would allow construction of a similar viscometer. No measurement of the radius  $R$  and only a nominal measurement of the length  $L$  would be necessary to obtain a sufficiently accurate value of  $R^4/L$ .

## Acknowledgments

Mike Moldover encouraged this work, and he pointed out the approximation for  $g_{\text{virial}}$ ; he also suggested recoiling the capillary to decrease  $R_{\text{curve}}$ . I thank David Cotrell and Geoff McFadden for identifying Yurun Fan, who graciously provided the accurate numerical calculations for  $De > 16$ . I acknowledge useful conversations with Anne Robertson, Harry Dwyer and Stanley Berger, and I thank Vitaliy Rayz for useful numerical calculations. John Hurly provided information about gas properties, Arno Laesecke identified much of the literature on centrifugal effects, Jim Schmidt provided the propane, and Ron Hartsock helped with the measurement of  $L$ . Antonio Jade of Scientific Glass Engineering provided useful information about the quartz capillary.

## Appendix A. Derivations of corrections for straight flow

### Appendix A.1. Virial correction

Generalize equation (3) to a non-ideal gas by substituting  $Q = \dot{n}/\rho$ , and integrate from entrance to exit of the capillary to obtain

$$-\frac{8M\dot{n}}{\pi R^4} \int_0^L dz = \int_{P_1}^{P_2} \frac{\rho}{\eta} dP. \quad (26)$$

Use the second and third pressure virial coefficients,  $B_P$  and  $C_P$ , to describe the gas's density as a function of pressure as

$$\rho = \frac{M}{R_{\text{gas}}T} \frac{P}{1 + B_P P + C_P P^2}. \quad (27)$$

Similarly, describe the viscosity as a function of pressure as follows:

$$\begin{aligned} \eta(T, \rho) &= \eta(T, 0) \left[ 1 + b \left( \frac{R_{\text{gas}}T\rho}{M} \right) + c \left( \frac{R_{\text{gas}}T\rho}{M} \right)^2 \right] \\ &= \eta(T, 0) \left[ 1 + \frac{bP}{1 + B_P P + C_P P^2} \right. \\ &\quad \left. + \frac{cP^2}{(1 + B_P P + C_P P^2)^2} \right] \\ &\cong \eta(T, 0) [1 + bP + (c - bB_P)P^2]. \end{aligned} \quad (28)$$

After substituting the descriptions of density and viscosity into equation (26) one obtains

$$\dot{n} = \dot{n} [1 + g_{\text{virial}}(P_1, P_2)], \quad (29)$$

where

$$\begin{aligned} g_{\text{virial}}(P_1, P_2) &\cong -(B_P + b)\bar{P} - [(C_P + c) - (B_P + b)^2] \\ &\quad \times \frac{P_1^2 + P_2^2}{2}. \end{aligned} \quad (30)$$

### Appendix A.2. Slip correction

**Appendix A.2.1. Slip length  $\zeta$ .** Applying the correction for slip in a circular duct at small  $Kn$  to equation (3) gives [11, 12]

$$Q(z) = -\frac{\pi R^4}{8\eta} \frac{dP}{dz} \left[ 1 + 4 \frac{\zeta(z)}{R} \right]. \quad (31)$$

Equation (31) expresses the volume flow rate  $Q(z)$  in terms of the local slip length

$$\zeta(z) \equiv - \left[ \frac{dv(r, z)/dr}{v(r, z)} \right]_{r=R}, \quad (32)$$

where  $v(r, z)$  is the velocity at radius  $r$  and longitudinal position  $z$ .

The slip length does not necessarily equal the molecular mean free path  $\lambda$ . Therefore, the purpose of the next two subsections is to derive an accurate relation between  $\zeta$  and  $\lambda$  in order obtain an accurate correction for slip flow (see also helpful references [39, 40]).

**Appendix A.2.2. Mean free path  $\lambda$ .** The concept of a mean free path is simple only for a hard-sphere gas. Thus, the mean free path is usually defined in terms of viscosity  $\eta$  instead of an effective molecular diameter  $\sigma$ . The mean free path for hard spheres in terms of  $\sigma$  is [41]

$$\lambda_{\text{HS}} = \frac{k_B T}{\sqrt{2} \pi \sigma^2 P}, \quad (33)$$

where  $k_B$  is the Boltzmann constant. The hard-sphere viscosity is

$$\eta_{\text{HS}} = \frac{5}{16} \frac{(\pi m k_B T)^{1/2}}{\pi \sigma^2} (1 + k_4), \quad (34)$$

where  $m$  is the molecular mass and  $k_4 = 0.01600$  accounts for collision-integral terms up to fourth order (see equation (19-14) in [41]) and equation (10.21,4) in [42]). Combining equations (33) and (34) gives

$$\lambda_{\text{HS}} = \frac{16}{5(1 + k_4)} \left( \frac{R_{\text{gas}}T}{2\pi M} \right)^{1/2} \frac{\eta_{\text{HS}}}{P}. \quad (35)$$

Table 4 gives three definitions of  $\lambda$  from the literature. An accurate slip correction requires a careful definition of  $\lambda$ . Using the wrong definition while assuming that  $\zeta = \lambda$ , as was done in [4, 17], can cause a slip error of 10%.

The present model adopts the definition of Loyalka and co-workers, namely

$$\lambda \equiv \left( \frac{2R_{\text{gas}}T}{M} \right)^{1/2} \frac{\eta}{P}. \quad (36)$$

**Appendix A.2.3. Ratio  $\zeta/\lambda$ .** The simplest assumption for the gas-wall interaction is full accommodation of momentum, so that a molecule leaving the surface has no memory of its previous velocity. Maxwell (see, e.g., [11]) related the slip length to the mean free path by assuming that the velocity gradient is uniform arbitrarily close to the wall. Then, for hard spheres,  $\zeta/\lambda_{\text{HS}} = 5\pi/16 = 0.98$ .

Modern calculations of the ratio  $\sigma_P = \zeta/\lambda$  are more accurate because they come from analytical or numerical solutions of the linearized Boltzmann equation. Analytical results can be found in Siewert and Sharipov [46], who used various model approximations to the linearized Boltzmann equation for hard spheres. Numerical results can be found in Loyalka and Hamoodi [44] and Wakabayashi *et al* [47].

The value of  $\sigma_P$  depends only weakly on the model approximation [43]. Siewert and Sharipov [46] found analytical values (for complete momentum accommodation) in the range  $0.967 < \sigma_P < 1.018$ . Their view is that the

**Table 4.** Definitions of the mean free path  $\lambda$ .

References	$\lambda/\lambda_{\text{HS}}$	
Loyalka and co-workers [43, 44]	$(2\pi^{1/2}) \frac{5\pi}{16} (1 + k_4)$	= 1.125 51
Sharipov and co-workers [39, 40, 45]	$\frac{5\pi}{16} (1 + k_4)$	= 0.997 46
Berg and Tison [4]	$(1 + k_4)$	= 1.016 00

best value for hard spheres is the numerical result [47]  $\sigma_P(\text{numerical}) = 0.9874$ . See also the discussion in [39].

The dependence of  $\sigma_P$  on the intermolecular potential also is weak. Loyalka [48] used Chapman–Enskog solutions for Lennard–Jones potentials fitted to several noble gases at 20 °C. He improved the Chapman–Enskog results  $\sigma_P(\text{CE})$  by multiplying them by the ratio  $\sigma_P(\text{numerical})/\sigma_P(\text{CE}) \cong 1.01$  for hard spheres. The resulting best estimates for He, Ar and Xe were, respectively, 0.996, 1.01 and 1.02. The range that comprises these values as well as the best hard-sphere value is

$$\sigma_P = \frac{\zeta}{\lambda} = 1.00 \pm 0.02. \quad (37)$$

The present model uses equation (37).

*Appendix A.2.4. Slip correction in terms of Kn.* The local slip length from equation (36) is

$$\lambda(z) = \left( \frac{2R_{\text{gas}}T}{M} \right)^{1/2} \frac{\eta(z)}{P(z)}. \quad (38)$$

Assume that the gas is ideal, rearrange equation (31), and integrate to obtain the molar flow rate,

$$\begin{aligned} \dot{n}_{\text{straight}} &= -\frac{\pi R^4}{8\eta L R_{\text{gas}} T} \left[ \int_{P_1}^{P_2} P \, dP - \frac{4K_{\text{slip}}}{R} \right. \\ &\quad \left. \times \int_{P_1}^{P_2} P \lambda(P) \, dP \right] \\ &= +\frac{\pi R^4}{8\eta L R_{\text{gas}} T} \left[ \frac{P_1^2 - P_2^2}{2} + 4K_{\text{slip}} \frac{\lambda_{1/2}}{R} \right. \\ &\quad \left. \times \frac{P_{1/2}}{\eta_{1/2}} \int_{P_1}^{P_2} \eta \, dP \right], \quad (39) \end{aligned}$$

where  $\lambda_{1/2}$  and  $\eta_{1/2}$  are the mean free path and viscosity at the ‘half’ pressure defined by  $P_{1/2} \equiv (P_1 + P_2)/2$ . Approximating the pressure-averaged viscosity in equation (39) by  $\eta_{1/2}$  gives

$$\dot{n}_{\text{straight}} = \dot{n}_0 [1 + 4K_{\text{slip}} Kn],$$

where  $Kn$  is defined by equation (8).

### Appendix A.3. Entrance correction

The increase in kinetic energy that occurs near the capillary’s entrance is accompanied by a small pressure drop,  $\Delta P_1 = K_{\text{ent}} \rho_1 \langle v^2 \rangle$ , where  $\langle v^2 \rangle$  is the squared velocity averaged over the duct’s cross section. The relative decrease in the volume flow rate is

$$\begin{aligned} \frac{\Delta Q_1}{Q_1} &= \frac{1}{Q_1} \frac{\pi R^4}{8\eta L} \left( \frac{1 + P_2/P_1}{2} \right) \Delta P_1 \\ &= \frac{1}{Q_1} \frac{\pi R^4}{8\eta L} \left( \frac{1 + P_2/P_1}{2} \right) K_{\text{ent}} \rho_1 \left( \frac{Q_1}{\pi R^2} \right)^2 \\ &= \frac{K_{\text{ent}}}{16} \left( \frac{1 + P_2/P_1}{2} \right) \frac{R}{L} Re. \quad (40) \end{aligned}$$

The value of  $K_{\text{ent}}$  has been measured and numerically calculated for capillary viscometers for liquids. To within 3%, the value  $K_{\text{ent}} = -1.14$  used here is consistent with the

values reported in [1] for  $100 < Re < 1500$ . For  $Re < 100$ , the uncertainty of  $K_{\text{ent}}$  is unimportant because the entrance correction is almost negligible.

### Appendix A.4. Expansion correction

One accounts for kinetic energy changes within the capillary by adding to equation (3) a ‘Bernoulli’ term equal to  $\rho \langle v^2 \rangle / 2$ . Equation (4) then becomes

$$Q_1 = Q_0 \left( \frac{1 + P_1/P_2}{2} \right) + \frac{\rho_1}{8\bar{\eta}L} Q_1^2 \ln \left( \frac{P_2}{P_1} \right). \quad (41)$$

Similar derivations have been used to describe gas flow through capillary viscometers of circular cross section [1]. (Several derivations made the error of using  $\langle v \rangle^2$  instead of  $\langle v^2 \rangle$  [5].) Approximating  $Q_1$  in the second term by the value of the first term yields an expansion correction similar to that in equation (2) but with the value  $K_{\text{exp}} = \frac{1}{2}$ . As shown by van den Berg *et al* [5], the correct value is  $K_{\text{exp}} = 1$  because gas expansion distorts the velocity profile from the assumed parabolic form. The resulting correction is

$$\dot{n}_{\text{straight}} = \dot{n}_0 \left[ 1 + \frac{K_{\text{exp}} R}{8L} Re \ln \left( \frac{P_2}{P_1} \right) \right]. \quad (42)$$

### Appendix A.5. Thermal correction

Van den Berg *et al* [6] derived an expression for the radial temperature distribution of the gas  $T_{\text{gas}}(r)$ . Their expression for the small difference between the cross-section-averaged gas temperature and the wall temperature  $T$  is

$$\langle T_{\text{gas}} \rangle - T = -\frac{2\eta}{3\kappa} (2T\alpha - 1) \langle v \rangle^2, \quad (43)$$

which gives the cooling in terms of the cross-section-averaged velocity  $\langle v \rangle$  and the gas properties, namely viscosity  $\eta$ , thermal conductivity  $\kappa$  and expansivity  $\alpha$ .

The cooler gas in the capillary’s interior increases the molar flow rate in two ways: by increasing the density and by decreasing the viscosity. Calculating the flow increase due to density requires averaging the temperature difference weighted by the parabolic flow profile. The resulting effective local temperature is

$$T_{\text{eff}}(z) = T \left[ 1 - \left( \frac{\eta}{\kappa T} \right) (2T\alpha - 1) \langle v(z) \rangle^2 \right]. \quad (44)$$

Calculating the flow increase due to viscosity starts from the estimate

$$\eta(r) = \eta + \left( \frac{\partial \eta}{\partial T} \right) [T_{\text{gas}}(r) - T] \quad (45)$$

for the position-dependent viscosity  $\eta(r)$ . One then inserts  $\eta(r)$  into the differential equation

$$\frac{1}{r} \frac{\partial}{\partial r} \left( r \eta(r) \frac{\partial v(r)}{\partial r} \right) = \frac{\partial P}{\partial z} \quad (46)$$

for Poiseuille flow in a circular pipe. This leads to an approximate expression for the volume flow rate in which



### Appendix B.2. Elliptical cross section

At small  $De$ , the impedance of a capillary with an elliptical cross section is [49]

$$Z = \frac{L}{2a^3b^3/(a^2 + b^2)}. \quad (55)$$

Measuring the cylinder's volume but assuming a circular cross section causes an impedance error given to lowest order in  $\varepsilon$  by

$$\frac{Z}{Z_{\text{volume}}} = 1 + \frac{\varepsilon^2}{2}. \quad (56)$$

At large  $De$ , estimating the impedance error due to ellipticity is more difficult. Srivastava's analytical calculation [50] indicates that a cross section with flatness  $\varepsilon > 0$  decreases the impedance ratio  $Z/Z_0$ . In other words, when ellipticity causes the cross section to bulge farther out of the plane of the coil as shown in figure 6, the centrifugal effect is less. A flatness of  $\varepsilon = 0.01$  causes a 0.03% impedance error at  $De = 10$ . The low order of Srivastava's calculation ( $De^4$ ) prevents accurate results at larger Dean numbers.

Numerical calculations by others [51–54] were valid at much larger  $De$ , but they used cross sections that were far from circular. Also, comparisons of the numerical results to each other and to van Dyke's calculation suggest that the uncertainty of any single result was never better than 1%. However, the results for a pair of ellipses from a single study can be subtracted to give a useful result if the ellipses have the same area but orthogonal orientations. For a flatness of  $|\varepsilon| \approx 0.3$ , such differences at  $De = 42$  [51] and  $60 < De < 260$  [54] have a sign that agrees with Srivastava's calculation, but their magnitudes do not exceed 3%. A linear extrapolation of this finding to small  $\varepsilon$  implies that, for  $|\varepsilon| < 0.01$ , the error due to ellipticity is less than 0.1% for  $De < 260$ . Random variations of the orientation of the ellipse that are likely to be present in a capillary coil will cause cancellations that reduce the error even further.

## Appendix C. Useful empirical correlations

### Appendix C.1. Van Dyke's theory for $f_{\text{cent}}(De, 0)$

Van Dyke's theory [8] yields a 12-term polynomial plus a logarithmic term in a variable derived from  $De$  by an Euler transformation. An iterative solution of the expression yields  $f_{\text{van Dyke}}(De) = f_{\text{cent}}(De, 0)$ . Remarkably, the much simpler expression

$$f_{\text{approx}}(De) = \left[ 1 + 16 \left( \frac{De}{De_0} \right)^4 \right]^{-1/16} \quad (57)$$

describes van Dyke's result at all Dean numbers to within 0.04%. The parameter

$$De_0 = \left[ \frac{(50\,400)(288)^2}{1541} \right]^{1/4} = 40.583\,85, \quad (58)$$

comes from the analytic solution in the limit of small  $De$ . (See van Dyke's footnote on p 132 of [8].) Equation (57) is useful

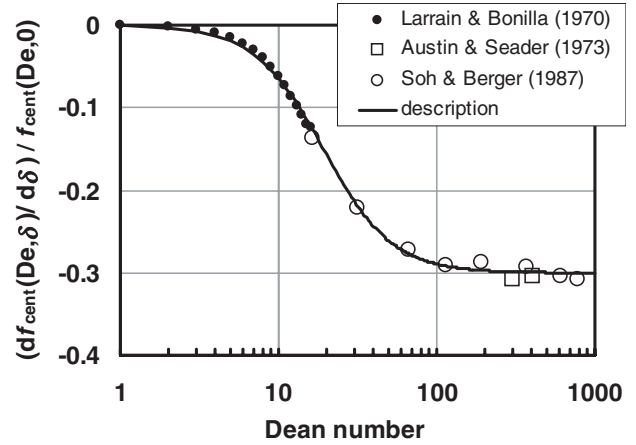


**Figure 7.** Normalized derivative of the centrifugal function with respect to the curvature ratio  $\delta$ .

for  $De < 120$  if an error of 1% is tolerable. Equation (57) also allows one to describe the normalized derivative as

$$\frac{De}{f_{\text{cent}}} \frac{\partial f_{\text{cent}}}{\partial De} \cong - \frac{4(De/De_0)^4}{1 + 16(De/De_0)^4}. \quad (59)$$

### Appendix C.2. Dependence of $f_{\text{cent}}(De, \delta)$ on the curvature ratio $\delta$

To lowest order, Larrain and Bonilla's analytical result for the centrifugal function has a quadratic dependence on the curvature ratio  $\delta = R/R_{\text{curve}}$ , but their result is valid only up to  $De = 16$ . Austin and Seader [55] and Soh and Berger [56] published numerical calculations at larger  $De$  and various values of  $\delta$ . Examination of their data revealed that, for  $De > 100$ , the normalized derivative  $[\partial f_{\text{cent}}(De, \delta)/\partial \delta]/f_{\text{cent}}(De, 0)$  has a simple linear dependence on  $\delta$  that is remarkably independent of  $De$ . The rational polynomial,

$$g_{\text{curve}}(De, \delta) = \frac{f_{\text{cent}}(De, \delta)}{f_{\text{cent}}(De, 0)} \cong 1 - \frac{a_\delta (De/De_\delta)^2 \delta}{1 + (De/De_\delta)^2}, \quad (60)$$

with  $a_\delta = 0.30$  and  $De_\delta = 19$ , matches the linear dependence at large  $De$  and approximates the quadratic dependence at small  $De$ . Figure 7 shows that equation (60) provides an adequate description at intermediate values of  $De$  also.

### Appendix C.3. Numerical results by Fan

Fan *et al* [9] used a toroidal coordinate system to calculate fully developed viscous and viscoelastic flows in curved pipes. Professor Fan recently used the same numerical code to calculate  $f_{\text{cent}}(De, \delta)$  in the range  $5 < De < 114$  [10]. The following function represents Fan's results (extrapolated to  $\delta = 0$ ) as a deviation from the simple function  $f_{\text{approx}}(De)$ .

$$g_{\text{dev}}(De) \equiv \frac{f_{\text{cent}}(De, \delta)}{f_{\text{approx}}(De) g_{\text{curve}}(De, \delta)} = \frac{1 + a \ln(1 + (De/De_0)^4) + b(De/De_0)^4}{1 + c(De/De_0)^4 + d(De/De_0)^6}. \quad (61)$$

The values  $a = -0.005\,964$ ,  $b = 0.2323$ ,  $c = 0.2251$  and  $d = 0.000\,967$ , describe Fan's results to within 0.01%.

## References

- [1] Kawata M, Kurase K, Nagashima A and Yoshida K 1991 *Capillary Viscometers, Measurement of the Transport Properties of Fluids* ed W A Wakeham *et al* (Oxford: Blackwell)
- [2] Berg R F 2004 Quartz capillary flow meter for gases *Rev. Sci. Instrum.* **75** 772–9
- [3] Berg R F and Tison S A 2004 Two primary standards for low flows of gases *J. Res. NIST* **109** 435–50
- [4] Berg R F and Tison S A 2000 Laminar flow of four gases through a helical rectangular duct *AICHE J.* **47** 263
- [5] van den Berg H R, ten Seldam C A and van der Gulik P S 1993 Compressible laminar flow in a capillary *J. Fluid Mech.* **246** 1
- [6] van den Berg H R, ten Seldam C A and van der Gulik P S 1993 Thermal effects in compressible viscous flow in a capillary *Int. J. Thermophys.* **14** 865
- [7] Larrain J and Bonilla C F 1970 Theoretical analysis of pressure drop in the laminar flow of fluid through in a coiled pipe *Trans. Soc. Rheol.* **14** 135
- [8] van Dyke M 1978 Extended Stokes series: laminar flow through a loosely coiled pipe *J. Fluid Mech.* **86** 129
- [9] Fan Y, Tanner R I and Phan-Thien N 2001 Fully developed viscous and viscoelastic flows in curved pipes *J. Fluid Mech.* **440** 327–57
- [10] Fan Y 2004 private communication
- [11] Kennard E H 1938 *Kinetic Theory of Gases* (New York: McGraw-Hill)
- [12] Thomson A L and Owens W R 1975 A survey of flow at low pressures *Vacuum* **25** 151
- [13] Dean W R 1927 Note on the motion of fluid in a curved pipe *Phil. Mag.* **20** 208
- [14] Dean W R 1928 The stream-line motion of fluid in a curved pipe *Phil. Mag.* **30** 673
- [15] Berger S A, Talbot L and Yao L-S 1983 Flow in curved pipes *Ann. Rev. Fluid Mech.* **15** 461
- [16] Jayanti S and Hewitt G F 1991 On the paradox concerning friction factor ratio in laminar flow in coils *Proc. R. Soc. Lond. A* **432** 291
- [17] Zohar Y, Lee S Y K, Lee W Y, Jiang L and Tong P 2002 Subsonic gas flow in a straight and uniform microchannel *J. Fluid Mech.* **472** 125–51
- [18] Batchelor G K 1967 *An Introduction to Fluid Mechanics* (Cambridge: Cambridge University Press) section 5.15
- [19] Trusler J P M 1991 *Physical Acoustics and Metrology of Fluids* (Bristol: Adam Hilger)
- [20] Matheson A J 1971 *Molecular Acoustics* (New York: Wiley)
- [21] Breshears W D and Blair L S 1973 Vibrational relaxation in polyatomic molecules: SF<sub>6</sub> *J. Chem. Phys.* **59** 5824–7
- [22] Kawata M, Kurase K, Yoshida K and Utsumi H 1971 Laminar flow and pressure drop in capillary tube *Flow, its Measurement and Control in Science and Industry* editor-in-chief R B Dowdell (Pittsburgh: Instrument Society of America) pp 17–26
- [23] Roark R J 1954 *Formulas for Stress and Strain* 3rd edn (New York: McGraw-Hill)
- [24] Mehl J B and Moldover M R 1982 Precondensation phenomena in acoustic measurements *J. Chem. Phys.* **77** 455
- [25] Suetin P E, Porodnov B T, Chernjak V G and Borisov S F 1973 Poiseuille flow at arbitrary Knudsen numbers and tangential momentum accommodation *J. Fluid Mech.* **60** 581
- [26] Porodnov B T, Suetin P E, Borisov S F and Akinshin V D 1974 Experimental investigation of rarified gas flow in different channels *J. Fluid Mech.* **64** 417
- [27] 1999 Design Institute of Physical Property Data (DIPPR), Project 801, Thermophysical Properties Laboratory, Brigham Young University, Provo UT 84602, <http://dippr.byu.edu/>
- [28] Lemmon E W, McLinden M O and Huber M L 2002 REFPROP database version 7.0, <http://www.nist.gov/srd/nist23.htm>
- [29] Miyamoto H and Watanabe K K 2000 A thermodynamic property model for fluid-phase propane *Int. J. Thermophys.* **21** 1045
- [30] Hurly J J, Defibaugh D R and Moldover M R 2000 Thermodynamic properties of sulfur hexafluoride *Int. J. Thermophys.* **21** 739
- [31] Vogel E 1984 Präzisionsmessungen des Viskositätskoeffizienten von Stickstoff und den Edelgasen zwischen Raumtemperatur und 650 K *Ber. Bunsenges. Phys. Chem.* **88** 997
- [32] Vogel E, Küchenmeister C, Bich E and Laesecke A 1998 Reference correlation of the viscosity of propane *J. Phys. Chem. Ref. Data* **27** 947
- [33] Strehlow T and Vogel E 1989 Temperature dependence and initial density dependence of the viscosity of sulphur hexafluoride *Physica A* **161** 101
- [34] Wakeham W A and Cole W A 1985 The viscosity of nitrogen, oxygen and their binary mixtures in the limit of zero density *J. Phys. Chem. Ref. Data* **14** 209
- [35] Hurly J J and Moldover M R 2000 *Ab initio* values of the thermophysical properties of helium as standards *J. Res. NIST* **105** 667–88
- [36] Łach G, Jeziorski B and Szalewicz K 2004 Radiative corrections to the polarizability of helium *Phys. Rev. Lett.* **92** 233001
- [37] Cencek W, Jeziorska M, Bukowski R, Jaszunski M, Jeziorski B and Szalewicz K 2004 Helium dimer interaction energies from Gaussian geminal and orbital calculations *J. Phys. Chem. A* **108** 3211–24
- [38] Hurly J J and Moldover M R 2004 private communication
- [39] Sharipov F and Seleznev V 1998 Data on internal rarified gas flows *J. Phys. Chem. Ref. Data* **27** 657
- [40] Sharipov F 2003 Application of Cercignani-Lampis scattering kernel to calculations of internal rarified gas flow. II Slip and jump coefficients *Eur. J. Mech. B Fluids* **22** 133
- [41] McQuarrie D A 1973 *Statistical Mechanics* (New York: Harper & Row)
- [42] Chapman S and Cowling T G 1970 *The Mathematical Theory of Non-Uniform Gases* (Cambridge: Cambridge University Press)
- [43] Loyalka S K and Ferziger J H 1967 Model dependence of the slip coefficient *Phys. Fluids* **10** 1833
- [44] Loyalka S K and Hamoodi S A 1990 Poiseuille flow of a rarefied gas in a cylindrical tube: solution of linearized Boltzmann solution *Phys. Fluids A* **2** 2061
- [45] Sharipov F and Seleznev V 1994 Rarefied gas flow through a long tube at any pressure ratio *J. Vac. Sci. Technol. A* **12** 2933
- [46] Siewert C E and Sharipov F 2002 Model equations in rarefied gas dynamics: viscous-slip and thermal-slip coefficients *Phys. Fluids* **14** 4123
- [47] Wakabayashi M, Ohwada T and Golse F 1996 Numerical analysis for the shear and thermal creep flows of a rarefied gas over the plane wall of a Maxwell-type boundary on the basis of the linearized Boltzmann equation for hard-sphere molecules *Eur. J. Mech. B/Fluids* **15** 175
- [48] Loyalka S K 1990 Slip and jump coefficients for rarified gas flows: variational results for Lennard-Jones and  $n(r)$ -6 potentials *Physica A* **163** 813
- [49] Lamb H 1932 *Hydrodynamics* 6th edn (New York: Dover)
- [50] Srivastava R S 1980 On the motion of a fluid in a curved pipe of elliptical cross-section *J. Appl. Math. Phys. (ZAMP)* **31** 297
- [51] Truesdell L C and Adler R J 1970 Numerical treatment of fully developed laminar flow in helically coiled tubes *AICHE J.* **16** 1010
- [52] Takami T and Sudou K 1984 Flow through curved pipes with elliptic cross sections *Bull. JSME* **27** 1176

- 
- [53] Dong Z F and Ebadian M A 1991 Numerical analysis of laminar flow in curved elliptic ducts *J. Fluids Eng.* **113** 555
- [54] Silva R J, Valle R M and Ziviani M 1999 Numerical hydrodynamic and thermal analysis of laminar flow in curved elliptic and rectangular ducts *Int. J. Therm. Sci.* **38** 585
- [55] Austin L R and Seader J D 1973 Fully developed viscous flow in coiled circular pipes *AIChE J.* **19** 85–94
- [56] Soh W Y and Berger S A 1987 Fully developed flow in a curved pipe of arbitrary curvature ratio *Int. J. Numer. Methods Fluids* **7** 733–55

# Erratum

## Simple flow meter and viscometer of high accuracy for gases

R F Berg 2005 *Metrologia* 42 11–23

Table 2 was incorrect due to a sign error of the viscosity ratios  $C_{N_2}$ (gas) and a misinterpretation of literature values for helium, nitrogen and argon. The corrected table is below. For helium, the corrected measured value differs from the *ab initio* calculated value of  $(19.823 \pm 0.006) \mu\text{Pa s}$  by twice the combined uncertainty of 0.05%.

**Table 1.** Values of the low density viscosity  $\eta_0$  at 25 °C obtained from the literature and from the present measurements. For optimum consistency, the measured values were derived only from flow measurements made with  $De < 20$  and  $P_2 \approx 100$  kPa, and the literature ratios were derived only from measurements made in a single laboratory (Vogel and co-workers). The absolute uncertainties of the last column correspond to a standard uncertainty of 0.037%.

Gas	$\eta_0$ (literature)/ ( $\mu\text{Pa s}$ )	$[C_{N_2}(\text{gas}) - 1] \times 100$	$\eta_0$ (present work)/ ( $\mu\text{Pa s}$ )
He	19.844 [31]	$+0.039 \pm 0.010$	$19.842 \pm 0.007$
N <sub>2</sub>	17.777 [31]	$0.000 \pm 0.010$	$17.762 \pm 0.007$
Ar	22.586 [31]	$+0.050 \pm 0.008$	$22.582 \pm 0.008$
C <sub>3</sub> H <sub>8</sub>	8.146 [18, 32]	$+0.162 \pm 0.010$	$8.148 \pm 0.003$
SF <sub>6</sub>	15.234 [28, 33]	$+0.076 \pm 0.009$	$15.226 \pm 0.006$